Dating deformation using crushed alkali feldspar: $^{40}Ar/^{39}Ar$ geochronology of shear zones in the Wyangala Batholith, NSW, Australia

Marnie Forster, Gordon Lister and Paul Lennox

Abstract Diffusion parameters have been estimated for K-feldspar in and adjacent to mylonite shear zones in the Wyangala Batholith. The parameters obtained suggest that deformation during mylonitization would have caused argon systematics to reset because diffusion distances were reduced by cataclasis, deformation and/or recrystallization. However, the mineral lattice remained sufficiently retentive to allow subsequently produced radiogenic argon to be retained. $^{40}Ar/^{39}Ar$ geochronology is thus able to constrain operation of these biotite-grade ductile shear zones to the period from ~380 Ma to ~360 Ma, at the end of the Tabberabberan Orogeny.

INTRODUCTION

Dating movement in shear zones is of particular interest to structural geology and tectonics, but timing something as intangible as movement can be difficult unless there are specific phenomena that can be attributed to the associated deformation. Processes such as recrystallization and/or the growth of new fabric forming minerals are candidate processes, for if there is new mineral growth, $^{40}Ar/^{39}Ar$ geochronology can be used to constrain its timing. However, the new grown minerals need to be sufficiently retentive of radiogenic argon to allow those ages to escape significant modification during subsequent events.

The technique can also work if deformation causes significant reduction in grain size, for example when micro-shear zones shred white mica until diffusion distances are small enough to allow rapid argon loss under the conditions that apply during shear zone operation. Again the modified material needs to remain sufficiently retentive of radiogenic argon to allow ages to escape significant modification during subsequent events. The question then arises as to what other processes might allow movement in shear zones to be dated using $^{40}Ar/^{39}Ar$ geochronology.

K-feldspar is a common rock-forming mineral, and it is commonly crushed and cataclased (± recrystallized) in ductile shear zones associated with the formation of mylonites. Perhaps crushed K-feldspar can also be used to date the timing of movement in shear zones? Forster & Lister (2009) tested this for the north-sense shear zones that overprint the South Cyclades Shear Zone, on Ios, Cyclades, Greece. The data obtained seem reliable, for the same age was determined from newly recrystallized white mica in the same shear zones, and from Rb-Sr measurements in adjacent calc-mylonites. In principle this result implies that $^{40}Ar/^{39}Ar$ K-feldspar geochronology could routinely be used to date the timing of movement in ductile shear zones. This hypothesis sets the background that led to the present study.

The Wyangala Batholith

There are spectacular mylonites and mylonitic shear zones in the Wyangala Batholith, especially in the Wyangala Dam region (Figure 1), with samples shown at thin section scale in Figure 2. We applied the same methods as reported by Forster & Lister (2009, 2010) to determine the timing of movement. Lennox *et al.* (2014) report these results in geological context.

Here we provide detail as to the method, and show how to analyze Arrhenius data. This documentation of procedure is important if we are to routinely date movement in ductile shear zones using these methods. The geology and tectonic setting of the samples analysed are described by Lennox *et al.* (2014).

These authors (*op. cit.*) report emplacement of the Wyangala batholith at ~425 Ma, in the mid- to late Silurian, and that this was followed by low- to medium-grade regional metamorphism (Cas 1983; Pogson & Watkins 1998; Glen 2005). Glen (2005, p. 55) noted the north-south elongation of this body and suggested this reflects Middle Devonian deformation "*with the formation of solid-state foliations and well developed S-C fabrics and mylonite zones*" (Vernon *et al.* 1983, *cf* Hobbs 1966). More detail as to the tectonic context can be found in Zee (1983), Morand (1988), Foster *et al.* (1999), Glen & Walshe (1999), Foster & Gray (2000) and Glen *et al.* (2007).

Samples were taken from two locations (Figure 1) so as to allow comparison of results from a mylonite with data from adjacent less intensely deformed proto-mylonite. The samples are: 1) a mylonite (sample PL336: grid reference 0679621m E, 6238053m N AGD84); and 2) a less deformed proto-mylonite adjacent to the mylonite zone (sample PL286: grid reference 0677794m E, 6236930 m N, AGD84). $^{40}Ar/^{39}Ar$ geochronology was undertaken on K-feldspar separated from both porphyroclasts and groundmass, for each sample.

The protolith is a granodiorite and comprises K-feldspar, plagioclase, biotite, quartz and sericite. The K-feldspar is preserved as microcline/perthite in abundant cm-scale porphyroclasts (CX) as well as within the groundmass (GM) where there are a significant number of smaller (<5 mm) grains (Figure 2). The K-feldspars both in the porphyroclasts and groundmass are relict from the magmatic crystallisation. Other K-rich minerals are small (<40 μm) and not readily suitable for analysis using $^{40}Ar/^{39}Ar$ geochronology.

Both the mylonite (PL336) and the less deformed proto-mylonite (PL286) were prepared for analysis by separately cutting out K-feldspar porphyroclasts and groundmass K-feldspars, providing four aliquots. These four K-feldspar samples were then crushed, sieved (size: >250 μm <420 μm, see Appendix 1), separated using heavy liquid, and then hand picked to ~99% purity, wrapped in aluminium foil, inserted into a canister with appropriate standards and other material used to determine correction factors, and submitted for irradiation. $^{40}Ar/^{39}Ar$ geochronology was conducted once the samples were returned, involving diffusion experiments on individual samples, with schedules of 34-36 heating steps between 450°C and 1450°C (tables and appendices in Lennox *et al.* 2014).

The experiments were carried out with a temperature-controlled furnace that allows precise control of temperature during step-heating. The step-heating experiments involved a minimum of two separate isothermal steps before the next sequence of isothermal steps was commenced, with peak temperature typically increased by ~30-50°C for each isothermal sequence. Lovera *et al.*

(1997) showed this procedure appears to minimise the effect of contaminating extraneous argon, and this is confirmed by our results (Figure 3).

The Arrhenius data (Figure 4) show that release of ^{39}Ar is systematic, and well approximated by diffusion theory, but the same is not true for the release of ^{40}Ar. This discrepancy suggests the existence of different microstructural gas reservoirs: i) one of these would be in the lattice and released by diffusion along with ^{39}Ar, while; ii) the other must be in sources such as adsorbed films or fluid inclusions. Extraneous argon may be released into high-diffusivity pathways as the result of decrepitation or other effects associated with temperature step increases. Figure 3 shows age oscillates when measuring gas released from two or more isothermal steps. These isothermal steps seem to allow 'cleaning' of the sample, so that if only the last step in each isothermal sequence is plotted age variation is smoothed (Figure 3b). Therefore only the last step of each isothermal sequence is utilised in our interpretation of the apparent age spectra (Figures 5 & 6).

Microstructural analysis shows that the difference between the K-feldspar in the mylonite compared to the less deformed granite is dominantly in the effects of cataclasis of the original K-feldspar porphyroclasts during ductile flow of the matrix. In the mylonite, naturally, there are many porphyroclastic grains that have undergone significant fracturing (Figure 2). Cataclasis has caused these larger grains to break into varying sized sub-grains, with internal deformation and twinning. More intense cataclasis occurs on the margins and at the ends of the porphyroclastic grains but these smaller sub-grains show little internal deformation. The relict K-feldspars in the groundmass also show little internal deformation (Figure 2).

Results from the step-heating experiments

The Arrhenius data were analysed so that the result is consistent with the Fundamental Asymmetry Principle (FAP) as described in Forster and Lister (2010). A spherical geometry was assumed for computation. The FAP requires division of the data by rank order. In practice this means that the first step or the last step in any isothermal sequence can be selected and that once a line is drawn joining the selected steps data, points that plot above the line precede those that plot below (Figure 4).

The FAP is a mathematical requirement for the analysis of multi-domain diffusion data, but assumes that activation energy does not vary amongst the domains releasing gas in the subset of data affected. It should be noted that this principle potentially allows many different estimates for the diffusion parameters to be made from a single Arrhenius plot. Forster & Lister (2010) demonstrated that the values obtained are always less than or equal to the actual diffusion parameters utilized in model simulations.

For estimates made for the intermediate-sized diffusion domains (plots on the left in Figure 4) application of the FAP meant in practice that the last step in one isothermal sequence was chosen (step 18 for example), and linked with the first step in each of the following three isothermal sequences (i.e., steps 19, 21, and 24). Parameters for intermediate-sized domains in these K-feldspar samples could thus be directly estimated, with results: i) for the proto-mylonite groundmass (Figure 4a) an activation energy of 78 kcal/mol, with closure at 443°C for a 20°C/Ma cooling rate; ii) for the proto-mylonite porphyroclasts (Figure 4c) an activation energy of 84 kcal/mol, with closure at 464°C for the same cooling rate; iii) for the mylonite groundmass (Figure 4e) an activation energy of 85 kcal/mol, with closure at 459°C; and iv) for the mylonite porphyroclasts (Figure 4g) an activation energy of 89 kcal/mol, with closure at 480°C. These values are sufficiently retentive to ensure that the argon systematics are likely to have been reset during deformation, but only if the K-feldspar in these biotite-grade shear zones was subject to temperatures exceeding ~440-480°C during mylonitization.

More difficult circumstances apply to points that can be used directly to estimate the diffusion parameters for the least retentive domains (see plots on the right in Figure 4). We have not selected the very first point because this seems anomalous. In general, the estimated value for D/a^2 decreases for each subsequent step in an isothermal sequence, both in practice and in theoretical simulations (Forster & Lister 2010). However this is not the case for the very first two steps which suggests that some ^{39}Ar loss may have occurred in the reactor in the lowest retentivity sites, e.g., as a result of recoil. The effect seems limited for it impacts only on the very first step. For practical purposes however, for this reason we do not consider the first step in applying the FAP.

Interpreted in this way the Arrhenius plots allow estimates for the diffusion parameters for the least retentivity diffusion domains as follows. For a 20°C/Ma cooling rate these least retentive domains: i) proto-mylonite groundmass (P1) closed at ~290°C by 285 Ma, with an activation energy of 60 kcal/mol (Figure 4b); ii) proto-mylonite porphyroclasts (P2) closed at ~288°C by 310 Ma, with an activation energy of 60 kcal/mol (Figure 4d); iii) mylonite groundmass (P3) closed at ~281°C by 285 Ma, with an activation energy of 58 kcal/mol (Figure 4f); and iv) mylonite porphyroclasts (P4) closed at ~286°C by 297 Ma, with an activation energy of 57 kcal/mol (Figure 4h). This means that the ductile-to-brittle transition must have taken place before 294 ± 12 Ma if movement in the shear zone was continuing. Note that although the activation energy directly estimated from the small domains is always less than the value estimated from the intermediate domains, this is a result that is consistent with the findings of modelling and simulation studies.

Forster & Lister (2010) show that any value obtained for the diffusion parameters in this way is always (mathematically) an underestimate. Hence the estimates made using data points from the low temperature steps can be discounted in favour of those made by extrapolating the results obtained for the domains with intermediate retentivity. The difference can be seen by comparing the results for the least retentive domains made by extrapolation (plots on the left in Figure 4) with the results for the least retentive domains obtained by applying the FAP directly (plots on the right in Figure 4). The plots on the right are in case less reliable because only two points could be selected while remaining consistent with the FAP (i.e. the Fundamental Asymmetry Principle of Forster and Lister, 2010).

The next step in this procedure is to compute r/r_0 plots using the method outlined in Lovera *et al*. (1989, 1997). These plots are shown in association with the apparent age spectra in Figures 5 & 6 since in that way we can determine (at least qualitatively) which domains are primarily responsible for the pattern of gas release. The temperature at which the least retentive domains would close (for cooling at a rate of 20°C/Ma) is in the range 280-290°C, while the median retentive domains would close (during cooling at the same rate) at temperatures in the range 440-480°C. Interestingly, all r/r_0 plots (Figures 5 & 6) show that each samples has a minor volume fraction (~5-10%) of diffusion domains up to 3 times larger than the median population. The estimates for the closure temperatures for these most retentive domains lie in the range 495-530°C, implying that these domains might not have been completely reset during the time of shear zone operation. These ages are almost certainly modified, but they could be relict from cooling immediately after emplacement of the granite.

The blue points in Figures 5 & 6 (in the online colour version) reflect steps in the heating sequence that bracket a plateau at the start of the period of main gas release. The red steps provide an age estimate for the upper limit of the time during which the median retentive domains were reset. These two limits thus potentially constrain the timing of movement. Coincidentally these same steps include steps in the Arrhenius plots that consistently allow application of the Fundamental Asymmetry Principle as they separate points on the plot according to rank order. Therefore we are able to provide independent estimates as to the retentivity of these diffusion domains, and as to the actual diffusion parameters. These data also show that the most retentive domains, reflecting ~10-20% of the volume of gas release, were sufficiently retentive as to prevent them being completely reset during the time of mylonitization. They may be thus responsible for relicts of older ages in the apparent age spectra (Figures 5 & 6).

In addition, the least retentive domains (Figures 5 & 6) are responsible for <~20% of the volume of gas release, and potentially reflect a fractal distribution of diffusion domain volume *versus* the radius of individual domains (*cf* models described in Forster & Lister 2010). These domains would have been completely reset during the period of mylonitization, because temperatures at that time exceeded ~400°C, because biotite remained stable. This part of the age spectra might thus reveal information as to the rate of cooling subsequent to the period of mylonitization and/or reflect the imprint of later lower temperature deformation, or other (unspecified) tectonothermal events.

Figures 5 & 6 show data from the groundmass K-feldspar in plots on the left, while plots on the right illustrate data from the porphyroclasts. Figure 5 is for the proto-mylonite samples (PL286-GM and PL286-CX), while Figure 6 is for the mylonite samples (PL336-GM and PL336-CX). Figures 5a, 5b, 6a & 6b show the full detail of the apparent age spectrum, while Figures 5e, 5f, 6e & 6f show the same data with the 'cleaning' steps removed. The two age limits mentioned above are computed from the data shown in Figures 5e, 5f, 6e & 6f.

Figures 5e, 5f, 6e & 6f readily allow definition of these bounding age limits (after Forster and Lister, 2004). The apparent age spectra, both from the groundmass from the porphyroclasts, rise to the lower limit: i) for the groundmass, at ~364 Ma for the proto-mylonite, and ~363 Ma for the mylonite; and ii) for the porphyroclasts, at 372 Ma for the proto-mylonite, and ~375 Ma for the mylonite. The apparent age spectra for the groundmass then display a staircase morphology, rising from ~364 Ma to ~375 Ma for the proto-mylonite and from 363 Ma to 380 Ma for the mylonite. The porphyroclasts display a rise from ~372 Ma to ~381 Ma for the proto-mylonite and 375 Ma to 396 Ma for the mylonite. The steps used are coloured: i) pale blue steps for the smallest diffusion domains; ii) dark blue steps for the intermediate-sized diffusion domains; and iii) red steps for the largest sized diffusion domains. Closure temperatures for the different diffusion domains are taken from Figure 4.

A plot of activation energy *versus* closure temperature, for a 20°C/Ma cooling rate is shown in Figure 7a and a plot of frequency factor *versus* activation energy is shown in Figure 7b. The dashed lines link data from porphyroclasts with data from the adjacent groundmass. The dotted lines link data for the intermediate-sized diffusion domains to those from the smallest diffusion domains, for each sample. Retentivity decreases from proto-mylonite to mylonite, implying that these parameters dynamically adjusted during deformation, thus fulfilling another of the requirements that would allow $^{40}Ar/^{39}Ar$ geochronology to date shear zone movement using crushed K-feldspar.

There is a systematic reduction in the estimated activation energy as deformation proceeds. Figure 7a shows high closure temperatures and high activation energies for all domains in both the mylonite and proto-mylonite rock, and shows a decrease in the mylonitised equivalent. Figure 7b plots the relation between activation energy and normalized frequency factor, and again shows this progression. Overall the range in closure temperature is from ~280°C in the smallest domains of the groundmass, to ~530°C in the most retentive domains of the porphyroclastic grains. The most represented domains (*i.e.* the intermediate domains) have closure temperatures that range from 440-480°C. The difference in size of these domains can be ascertained from the r/r_0 plots in Figures 5c, d & 6c, d, which show that the small domains are up to 1000 times smaller.

Results from modelling and simulation using MacArgon

Comparison of r/r_0 plots with apparent age spectra is qualitatively of value, but to obtain more exact constraints it is necessary to undertake modelling and simulation. To do this we used the *MacArgon* program (by now extensively modified from that originally reported by Lister & Baldwin 1996) to constrain the range of end member temperature-time histories capable of producing apparent age spectra bracketing the variation evident in the natural samples.

To demonstrate this we used the diffusion parameters inferred from sample PL286-CX (see Figure 4c). The volume ratios are those that can be estimated from the corresponding r/r_0 plot (Figure 5d). The data for the median retentive domains reflect a consistent ~60-70% of the volume of ^{39}Ar released, and diffusion domains have a retentivity that would allow them to have been reset during the period of mylonitization.

Temperature-time histories are input parametrically until bounds on feasible end-member temperature-time histories can be ascertained. If diffusion domains with a volume-size distribution as can be estimated from the r/r_0 plot are utilised, the temperature-time history illustrated in Figures 8a & 8c produce age spectra as illustrated in Figures 8b & 8d. The variation that is obtained by simulation of the effects of these end-member temperature-time histories replicates that which is observed in the measured spectra (Figures 5 & 6).

It was also demonstrated that unless overall gradual cooling was assumed (Figures 8a & 8c), the pattern of age variation between the most retentive and least retentive diffusion domains would be inconsistent. Interestingly, however, cooling during the period of mylonitization (Figure 8a) was required in order to produce staircase spectra for the median domains, with ages ranging from 365-375 Ma (Figure 8b). Branching fractal volume-radius distributions improve the quality of the fit, but these simulations are not reported here.

Discussion

The method described here requires that $^{40}Ar/^{39}Ar$ geochronology be conducted during step-heating experiments conducted *in vacuo,* during which time the ^{39}Ar produced during neutron irradiation of the sample prior to measurement is progressively outgassed. The method also requires volume release data and Arrhenius plots that allow the range of relative diffusion domain sizes to be constrained, along with the corresponding estimates of the diffusion parameters (Lovera *et al*. 1989, 1997). $^{40}Ar/^{39}Ar$ geochronology can date the timing of movement if 'closure temperatures' for the range of diffusion domains in the cataclased K-feldspar bracket the time-temperature conditions of mylonitization.

If we want to demonstrate that this method has the potential to be able to estimate the timing of movement, it is critical that we demonstrate the existence of relatively retentive diffusion domains in the K-feldspar in question. We must also show that the temperature conditions during mylonitization were sufficient to allow such domains to have been reset at the temperatures at which movement took place. It is also necessary to show that these domains were sufficiently retentive so as to close (to argon diffusion) soon after deformation stopped, as the rock mass began to cool.

These three conditions may routinely apply to crushed and cataclased K-feldspar in mylonitized granitoids. Quartz microstructures in such rocks typically attest to the effects of dynamic recrystallization. These microstructures (along with the accompanying argon ages) must have been frozen into the rock as we see it today shortly after deformation ceased. Otherwise the microstructure would have been significantly modified by recrystallization and grain growth. Rapid cooling should also be expected once mylonite activity has ended, because conductive relaxation ensures that dynamically created perturbations to the geotherm are speedily erased once movement in a mylonite zone ceases. Granitoids mylonitized under biotite-grade greenschist facies therefore potentially (routinely?) should allow $^{40}Ar/^{39}Ar$ geochronology to extract constraints as to the timing of microstructural modification caused by cataclasis and grain-scale comminution (of K-feldspar).

The critical aspect is to be able to demonstrate the retentivity of the diffusion domains, and the link between mylonitization and the diffusion dimensions. We do not imply that there is a correspondence between grain size and the dimensions of individual diffusion domains however. Clearly, as shown by the data (Figure 7), mylonitization does appear to influence the diffusion domain dimensions, and makes them less retentive. But there is no substantive difference between matrix grains and porphyroclasts in terms of their relative diffusion dimensions. The collection of Arrhenius data during step-heating experiments *in vacuo* is essential to allow quantification of this aspect. Otherwise independent assessment of retentivity is not possible, and the method cannot be rigorously applied.

There are also certain theoretical principles that need be followed in the analysis of the Arrhenius data (Forster & Lister 2010). For example when all diffusion domains have the same activation energy the Fundamental Asymmetry Principle (FAP) must be obeyed if self-consistent analysis of Arrhenius data is to be undertaken. How the FAP is applied in the analysis of Arrhenius data has been illustrated. Correct (?) analysis of the Arrhenius data is an essential element in the application of this method.

Comparison with previous results

Ages of ~380-370 Ma have been obtained from $^{40}Ar/^{39}Ar$ dating of metamorphic biotite in similar and/or adjacent bodies (Lennox *et al.* 1998; Foster *et al.* 1999; Glen *et al.* 1999). Lennox *et al.* (1998) report a biotite age from the S-type Sunset Hills Granite using furnace step heating experiments. They report an average age of 371± 2 Ma, with the age for each step falling in the range 363 - 379 Ma. Foster *et al.* (1999) report a 383 ± 3 Ma age from a biotite sample taken from a shear zone in the Wyangala Batholith. These results might therefore be taken as indistinguishable from our own.

The $^{40}Ar/^{39}Ar$ apparent age spectra (Figures 5 & 6) show that similar ages were obtained during the main period of gas release, while the median retentivity diffusion domains degassed. The details of the gas release before and after show slightly different patterns, however. Groundmass K-feldspar shows relict ages, up to ~395 Ma, for example. The simulations show that the preservation of these (albeit strongly modified) relict ages could have important implications, namely reheating during the period of mylonitization.

While the median retentivity domains in the porphyroclastic feldspars preserve 'plateau' ages of 372-375 Ma, the groundmass K-feldspar in the proto-mylonite rock (PL286-GM) yields ages that progressively decrease to ~365 Ma. Groundmass K-feldspar shows only slightly younger ages. These domains are not so retentive as to have prevented argon systematics from being almost completely reset in these diffusion domains during deformation, so these are cooling ages which demonstrate when the rock mass cooled beneath temperatures that allow ductile behaviour.

Overall the apparent age spectra show a pattern of argon release typical of that expected in samples that have suffered argon loss as the result of solid-state diffusion. The age spectra initially rise towards a limit that can be defined by first release of gas from the median retentive domains. The bulk of the gas is then released, but release of gas from more retentive domains increasingly also begins to takes place. The staircase form of the apparent age spectra is to be expected because the range of diffusion parameters brackets conditions that would allow almost no retentivity, whereas some larger diffusion domains would be capable of retaining older ages. This distribution of diffusion dimension can be seen in the r/r_0 plots (Figures 5 & 6, *cf* Lovera *et al.* 1997).

Is K-feldspar an unretentive mineral?

Uncertainty is introduced by disagreement as to how Arrhenius data should be analysed. However the inference of unretentive parameters leads inexorably to claims as to the existence of short duration thermal events, e.g., Baldwin &

Lister (1998) showed their data required thermal pulses no longer than 0.01-0.1 Ma. Conductive heat transport implies a quadratic relation between time and length scales (*e.g.*, Viete *et al*. 2012) so such brief thermal excursions imply heat sources that should be sufficiently proximal so as to be observed on the scale of an outcrop. This is not the case.

This riddle was resolved only when Forster & Lister (2009) showed that by obeying the FAP, more retentive values for the diffusion parameters are obtained. These more retentive diffusion parameters do not require extremely short duration thermal events to have taken place. Modelling and simulation showed that these more retentive estimates imply that K-feldspar can retain relatively old apparent ages, even during prolonged (five million year duration) heating events. In the case of the South Cyclades Shear Zone ductile deformation took place during biotite-grade greenschist facies conditions, at temperatures estimated to lie between 400-450°C. The longer time-scale estimates are consistent with thermal behaviour expected at such depths.

K-feldspar has been labelled in the past as a relatively unretentive mineral that readily loses radiogenically produced argon in the natural environment. We argue that data such as that above suggest this is perhaps an unwarranted assumption. Indeed, if K-feldspar is generally more retentive than has been previously assumed, we can resolve geodynamic issues associated with the inference of unreasonably short thermal events.

For example by assuming more retentive diffusion parameters we are able to resolve the dilemma faced by Burgess *et al.* (1992). These authors used data from Foland (1974) for argon diffusion in orthoclase, where, assuming cooling at 10°C/Ma, closure takes place around 240°C for 100 μm grains. They were thus forced to conclude that the maximum temperature experienced by their sample, from the Klokken Syenite, did not exceed 240°C for the billion or so years since emplacement and initial cooling of this igneous body. If there was a thermal excursion, the unretentive diffusion parameters they use require that any such event could not have endured for >1 Ma. More retentive K-feldspar provides more reasonable answers in that longer time scales can be considered, and higher temperatures.

Conclusions

The timing of movement in mylonite shear zones potentially can be dated using cataclased K-feldspar. The Arrhenius data obtained for the Wyangala samples imply closure temperatures of ~440-480°C for a 20°C/Ma cooling rate. Since the shear zones formed under conditions that allowed K-feldspar porphyroclasts to be wrapped by biotite-muscovite-hornblende composites, it is reasonable to assume that deformation occurred at temperatures in the range 400°C-500°C.

Modelling and simulation demonstrate two scenarios with temperature-time variation capable of reproducing the age spectra from the samples analysed: i) cooling after emplacement of a granite body, with the cooling rate accelerating during the period of shear zone operation; and ii) a thermal pulse superimposed on a cooling curve. The accelerated cooling model involves a change from cooling at ~22°C/Ma from 550°C at 380 Ma, to a cooling rate of ~110°C/Ma for 20 million years, until temperature drops to ~330°C at 360 Ma. The thermal pulse model requires temperatures rise, but to no greater than 500°C at 380 Ma, and maintained temperatures between 470-500°C until 365 Ma. Rapid cooling then takes place with temperature reaching 330°C by 360 Ma.

All models require reduction in diffusion dimension during mylonitization, to allow argon systematics to be reset. The models also require rapid cooling from ~365 Ma, with temperature reaching 330°C by 360 Ma, in order to simulate the age variation in the least retentive domains. Importantly, the thermal pulse model shows that the medium retentivity domains cannot retain ages older than 365 Ma if the thermal pulse is maintained at a constant temperature of 500°C, from 380 to 365 Ma (Figure 8d). The observed spread of ages in the median retentive domains can be simulated if peak temperatures are ~480°C however. This thermal pulse scenario does allow the high retentivity domains to retain ages up to 395 Ma, where this is not a feature of the accelerated cooling model. Variation within the bounds defined by these two temperature-time histories overall produces results consistent with the measured apparent age spectra.

The Arrhenius data imply increased diffusivity during deformation, presumably as the result of grain comminution or in consequence of recrystallization of K-feldspar grains. The smallest domains are unretentive, as expected (see Lovera *et al.* 1989; 1997), but appear to retain information as to how slowly the terrane cooled beneath 330-340°C. The largest domains are more retentive and provide important control on the type of temperature-time history that can be inferred. Cooling is required during the temperature interval reflected in microstructures produced by ductile deformation within the shear zones

Microstructures show that cooling was taking place while the mylonite continued to deform, and this cooling during ongoing deformation resulted in both the age (and the microstructure) being frozen into the rock. If matters were otherwise, microstructures typical of dynamic recrystallization during cooling from 500°C to 450°C would not be evident in quartz aggregates. Because this is so, and because the range of retentivity inferred for the intermediate sized domains allows resetting during mylonitization, $^{40}Ar/^{39}Ar$ geochronology on the samples of K-feldspar from the Wyangala shear zones directly records the timing of deformation ± recrystallization.

Acknowledgments

M.A. Forster acknowledges an Australian Research Fellowship provided by the Australian Research Council (ARC) and ARC Discovery Grant DP0877274 “Tectonic mode switches and the nature of orogenesis”. P. Lennox acknowledges the support of a UNSW Faculty of Science Research Grant. Irradiations were done at the USGS TRIGA reactor, Denver, USA. $^{40}Ar/_{39}Ar$ analysis was done at the RSES Argon Facility, ANU. Samples were collected by P. Lennox and K. Czarnota. Mineral separation done by L. White and S. Paxton.

References

Baldwin S. L. & Lister G.S. 1998. Thermochronology of the South Cyclades shear zone, Ios, Greece: effects of ductile shear in the argon partial retention zone. *Journal of Geophysical Research* **103** 7315–7336.

Burgess R., Kelley S.P., Parsons I., Walker F.D.L., Worden R.H. 1992. ^{40}Ar-^{39}Ar analysis of perthite microtextures and fluid inclusions in alkali feldspars from the Klokken syenite, South Greenland. *Earth and Planetary Science Letters* **109**: 147-1.

Cas R.A.F. 1983. A review of facies patterns, palaeogeographic development and tectonic context of the Palaeozoic Lachlan Fold Belt of southeastern Australia. *Geological Society of Australia Special Publication* **10**.

Foland K.A. 1974. ^{40}Ar diffusion in homogeneous orthoclase and an interpretation of Ar diffusion in K-feldspars, *Geochimica et Cosmochimica Acta* **38**, 151-166.

Forster M.A. & Lister G.S. 2004. The interpretation of ^{40}Ar/^{39}Ar apparent age spectra produced by mixing: application of the method of asymptotes and limits. *Journal of Structural Geology* **26**, 287-305.

Forster M.A. & Lister G.S. 2009. Core complex related extension of the Aegean lithosphere initiated at the Eocene-Oligocene transition. *Journal of Geophysical Research (Solid Earth)* **114***,* B02401, doi:10.1029/2007JB005382.

Forster M.A. & Lister G.S. 2010. Argon enters the retentive zone: reassessment of diffusion parameters for K-feldspar in the South Cyclades Shear

Zone, Ios, Greece. *In:* Advances in interpretation of geological processes: refinement of multi-scale data and integration in numerical modelling. *Geological Society, London, Special Publication* **332,** 17-34. doi:10.1144/SP332.2

FORSTER M.A. & LISTER G.S. 2013. $^{40}Ar/^{39}Ar$ geochronology and the diffusion of ^{39}Ar in phengite-muscovite intergrowths during step-heating experiments in vacuo. In: Advances in $^{40}Ar/^{39}Ar$ Dating: from Archaeology to Planetary Sciences, Eds. Jourdan, F., Mark, D.F. and Verati, C. *Geological Society, London, Special Publications,* **SP378.** doi:10.1144/SP378.

FOSTER D., GRAY D.R., & BUCHER M. 1999. Chronology of deformation within the turbidite-dominated, Lachlan orogen: Implications for the tectonic evolution of eastern Australia and Gondwana. Tectonics **18**, 452-485. DOI: 10.1029/1998TC900031

FOSTER D. & GRAY D. 2000. Evolution and structure of the Lachlan Fold Belt (Orogen) of eastern Australia. *Annual Review Earth Planetary Sciences*, **28**, 47–80.

GLEN R.A. 2005. The Tasmanides of eastern Australia. *Geological Society, London, Special Publications* **246**, 23-96. Doi: 10.1144/GSL.SP.2005.246.01.02

GLEN R.A. & WALSHE J. L. 1999. Cross-structures in the Lachlan Orogen: the Lachlan Transverse Zone example. *Australian Journal of Earth Sciences* **46**:, 385-415. DOI:10.1080/08120090601147019

GLENN R.A., LENNOX P.G. & FOSTER D.A. 1999. ^{40}Ar-^{39}Ar dating of deformations west of the Hill End Trough, Lachlan Orogen, New South Wales. *Quarterly*

Notes of the Geological Survey of New South Wales, **II0**, 13-22.

Glen R.A., Meffre S. & Scott R.J. 2007. Benambran Orogeny in the Eastern Lachlan Orogen, Australia. *Australian Journal of Earth Sciences* **54**:, 385-415. DOI:10.1080/08120090601147019

Hobbs B.E. 1966. Microfabrics of tectonites from the Wyangala Dam area, New South Wales, Australia. Geological Society of America Bulletin **77**, 685-706.

Lister G.S. & Baldwin, S.L. 1996. Modelling the effect of arbitrary P-T-t histories on argon diffusion in minerals using the MacArgon program for the Apple Macintosh. *Tectonophysics* **253**, 83-109.

Lennox P., Fowler T. & Foster D. 1998. The composite Barry Granodiorite and Sunset Hills Granite: Wyangala-style intrusion at the margin of a regional ductile shear zone, northern Lachlan Fold Belt, New South Wales, *Australian Journal of Earth Sciences* **45**, 849-863. DOI: 10.1080/08120099808728440

Lennox P.G., Forster, M.A. & Williams, I.S. 2014. Emplacement and deformation ages of the Wyangala Granite, Cowra, NSW. *Australian Journal of Earth Sciences*, in review, accepted with minor revisions.

Lovera O.M., Richter F.M. & Harrison T.M. 1989. The 40Ar/39Ar thermochronometry for slowly cooled samples having a distribution of diffusion domain sizes. *Journal of Geophysical Research* **94**, 17,917–17,935.

Lovera O.M., Grove M., Harrison T.M. & Mahon, K.I. 1997. Systematic analysis of K-feldspar 40Ar/39Ar step heating results: I. Significance of activation energy determinations. *Geochimica et Cosmochimica Acta* **61**, 3171-3192.

Morand V.J. 1988. Emplacement and deformation of the Wyangala batholith, New South Wales. *Australian Journal of Earth Sciences* **35**, 339-353.

Paterson S.R., Tobisch O.T. & Morand V.J. 1990. The influence of large ductile shear zones on the emplacement and deformation of the Wyangala Batholith, SE Australia. *Journal of Structural Geology* **12**, 639-650.

Pogson D.J., Watkins J.J. 1998. Bathurst 1:250 000 geological Sheet. SI/55-8: Explanatory Notes. Australian Geological Survey Organisation and Geological Survey of New South Wales SI/55-8

Vernon R.H., Williams V.A. & D"Arcy W.F. 1983. Grain-size reduction and foliation development in a deformed granitoid batholith. *Tectonophysics*, **92**, 123-145.

Viete D., Oliver G.J.H., Fraser G.L., Forster M.A., Lister G.S. 2013. The nature and origin of the Barrovian metamorphism, Scotland: $^{40}Ar/^{39}Ar$ apparent age patterns and the duration of metamorphism in the biotite zone. *Geological Society, London, Special Publication* **168,** 133-146.

Zee R.Y.S. 1983. Structural development of the Wyangala area, central New South Wales, Australia. BSc(Hons) thesis. Monash University.

Figure Captions

Figure 1 Location map of samples from the Wyangala Batholith at Wyangala Dam, NSW, Australia. Sample PL336 (336) is located within a high-strain mylonite shear zone at Wyangala Dam (defined as light grey zones trending ~N-S on the eastern margin of the Batholith). Sample PL286 (286) is located ~1 km west of the dam away from the most intense fabrics of the mylonite zone. The grid reference (AGD84) for sample PL286 is 0677794m E, 6236930m N while that for sample PL336 is 0679621m E, 6238053m N.

Figure 2 Microphotographs of samples: (a) the proto-mylonite; and (b) the mylonite. In (a) the sampled groundmass (P1) grains are distortion-free, and bounded by microshear zones defined by quartz and mica, while the sampled porphyroclastic K-feldspar (P2) is preserved as single grains with twinning and minor crushing and fracturing of grains. The mylonite (b) has undergone considerably greater deformation, but again the sampled groundmass K-feldspar (P3) does not show significant distortion, and grains are wrapped by ribbon quartz and fine-grained mica that define the mylonite foliation, while the sampled K-feldspar porphyroclasts (P4) are intensely faulted and cataclased.

Figure 3 Plots on the left show the apparent age spectra for the four samples measured, with the horizontal scale expanded to show the detail in the first 20% of gas release (a, c, e, g). Plots on the right (b, d, f, h) show the same data but with the ‘cleaning’ step eliminated. This method reduces scatter and oscillatory behaviour, and produces more systematically varying apparent age spectra.

Figure 4 Analysis of the Arrhenius data from the step-heating experiments, showing estimates calculated using a spherical geometry. The plots on the left (a, c, e & g) are estimates for the intermediate sized diffusion domains, while the plots on the right (b, d, f & h) are for the smallest-sized domains. The plots on the right are less reliable because only two points could be selected while remaining consistent with the Fundamental Asymmetry Principle (FAP) of Forster & Lister (2010). The FAP is a mathematical requirement for the analysis of multi-domain diffusion data, but assumes that activation energy does not vary amongst the domains releasing gas in the subset of data affected. The FAP requires division of the data by rank order, *i.e.*, the first or the last step in any isothermal sequence, with the selected step numbers as shown. The activation energy estimated from the small domains is always less than the value estimated from the intermediate domains, consistent with the findings of modelling and simulation studies (Forster & Lister 2010). Data for intermediate-sized domains in K-feldspar: (a) proto-mylonite groundmass, activation energy 78 kcal/mol with closure for 20°C/Ma cooling rate at 443°C; (c) proto-mylonite porphyroclasts, activation energy 84 kcal/mol with closure at 464°C; (e) mylonite groundmass, activation energy 85 kcal/mol with closure at 459°C; and (g) mylonite porphyroclasts, activation energy 89 kcal/mol with closure at 480°C. The least retentive domains (see plots on the right) close at 281-290°C, requiring the ductile-to-brittle transition to have taken place, if movement was continuing.

Figure 5 $^{40}Ar/^{39}Ar$ apparent age spectra for K-feldspar: (a) groundmass from the proto-mylonite sample PL286-GM; (b) porphyroclasts from the proto-mylonite sample PL286-CX, with step-heating sequences involving 36 steps. The next step in the data analysis is examination of the spectrum of relative diffusion domain sizes, shown in r/r_0 plots (c) and (d) calculated using equations in Lovera *et al*. (1989, 1997). These allow recognition of the steps in the apparent age spectrum most influenced by gas release from the intermediate- versus the largest-sized diffusion domains. Data from cleaning steps are eliminated in apparent age spectra shown in (e) and (f) and bounding limits (after Forster and Lister, 2004) are thereby defined. It can be then seen that the apparent age spectra, both from the groundmass from the porphyroclasts, rise to an intermediate limit, for the groundmass at ~364 Ma, and the porphyroclasts at ~372 Ma. The apparent age spectra then display a staircase morphology, from ~362 Ma to ~375 Ma for the groundmass, and from ~372 Ma to ~381 Ma for the porphyroclasts. Note the single step at 388 Ma is a relict outlier. The steps used are: i) pale blue for the smallest diffusion domains; ii) dark blue for the intermediate-sized diffusion domains; and iii) red for the largest sized diffusion domains. Closure temperatures for these different diffusion domains are shown in Figure 4.

Figure 6 $^{40}Ar/^{39}Ar$ apparent age spectra for K-feldspar: (a) groundmass from the mylonite sample PL336-GM; (b) porphyroclasts from the mylonite sample PL336-CX, with step-heating sequences involving 36 and 34 steps respectively. The apparent age spectrum from the groundmass displays a classic staircase morphology, from ~363 Ma to ~380 Ma, over 60% of the gas released. The apparent age spectrum from the porphyroclasts rises asymptotically to an intermediate limit, at ~375 Ma. This is a plateau segment defined by ~25% of gas release. The next step in the data analysis is examination of the spectrum of relative diffusion domain sizes, shown in r/r_0 plots (c) and (d) calculated using equations in Lovera *et al*. (1989, 1997). These allow recognition of the steps in the apparent age spectrum most influenced by gas release from the intermediate- versus the largest-sized diffusion domains. Data from cleaning steps are eliminated in apparent age spectra shown in (e) and (f) and bounding limits (after Forster and Lister, 2004) are thereby defined. The steps used are coloured: i) pale blue steps for the smallest diffusion domains; ii) dark blue steps for the intermediate-sized diffusion domains; and iii) red steps for the largest sized diffusion domains. Closure temperatures for these different diffusion domains are shown in Figure 4.

Figure 7 Activation energy *versus* closure temperature, for a 20°C/Ma cooling rate (a); and frequency factor *versus* activation energy (b). The dashed lines link data from porphyroclasts with data from the adjacent groundmass. The dotted lines link data for the intermediate-sized diffusion domains to those from the smallest diffusion domains, for each sample. Retentivity decreases from proto-mylonite to mylonite, implying that these parameters dynamically adjusted during deformation.

Figure 8 *MacArgon* simulations of the effect of end-member temperature-time (T-t) paths that bracket the variation in age spectra from the samples analyzed. Accelerated cooling (from 550°C at 380 Ma to 330°C at 360 Ma) during the period of shear zone operation (a, b) could take place because conduction quickly relaxes local perturbations in the geotherm, but this type of T-t path cannot explain preservation of older relict ages in the most retentive domains. It does allow explanation of staircase apparent age spectra rising from 365 Ma to 375 Ma, however. In (c, d) we superimpose a temperature pulse on the cooling history, beginning at 380 Ma, rising to 500°C, with that temperature maintained for 15 million years. The thermal perturbation is completely ended by 360 Ma. This type of history needs a deeper magma source to explain the temperature rise, and allows preservation of older ages in the most retentive domains (d). However if temperature rises to 500°C and then abruptly falls, as shown, the staircase spectra from 375 Ma to 365 Ma are eliminated. Diffusion parameters and domain size variation are those inferred from sample PL286-CX.

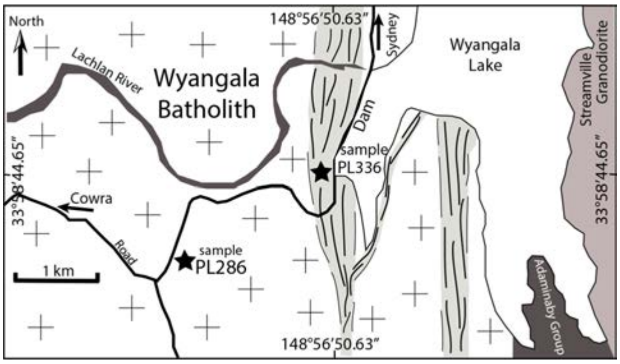

Figure 1

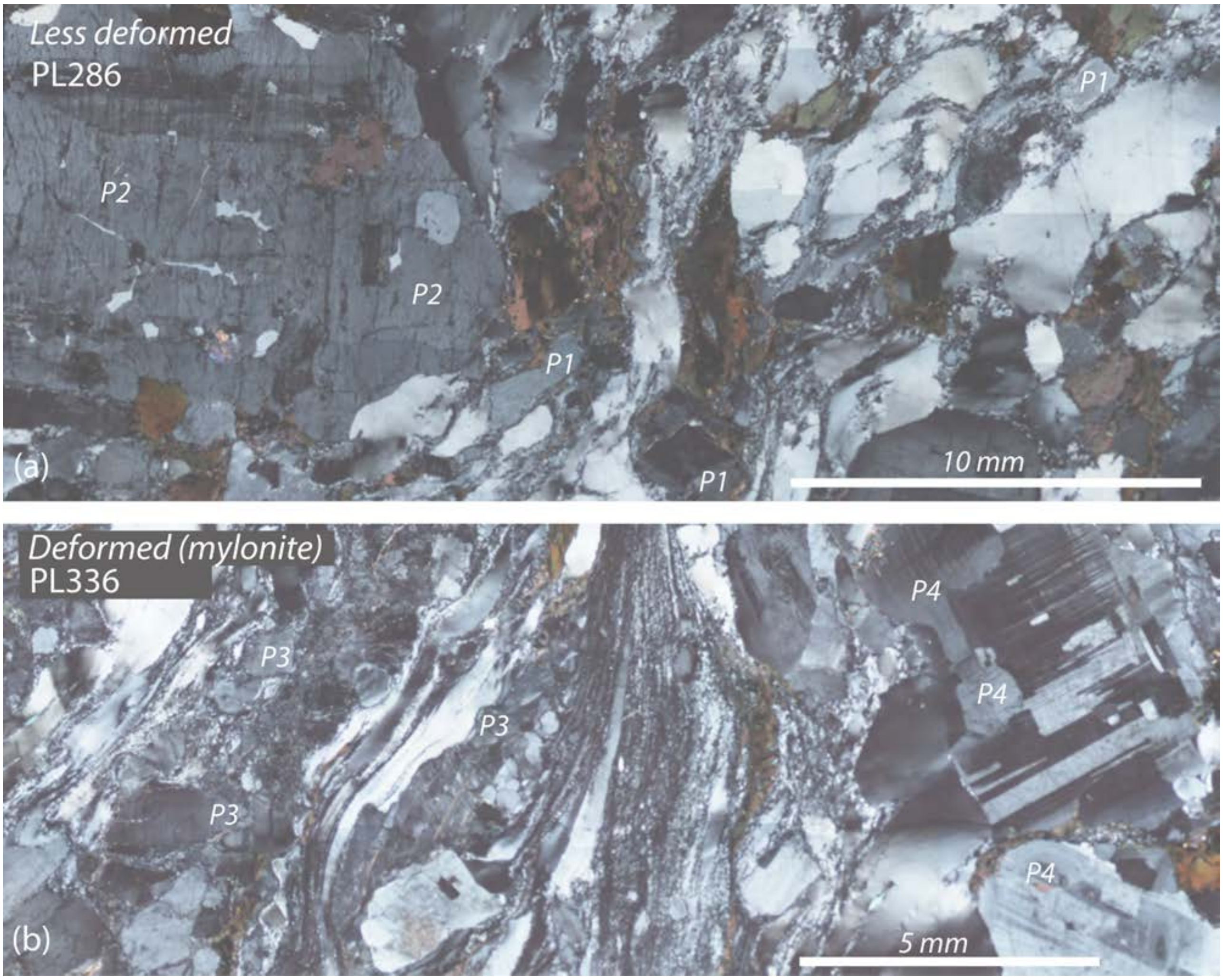

Figure 2

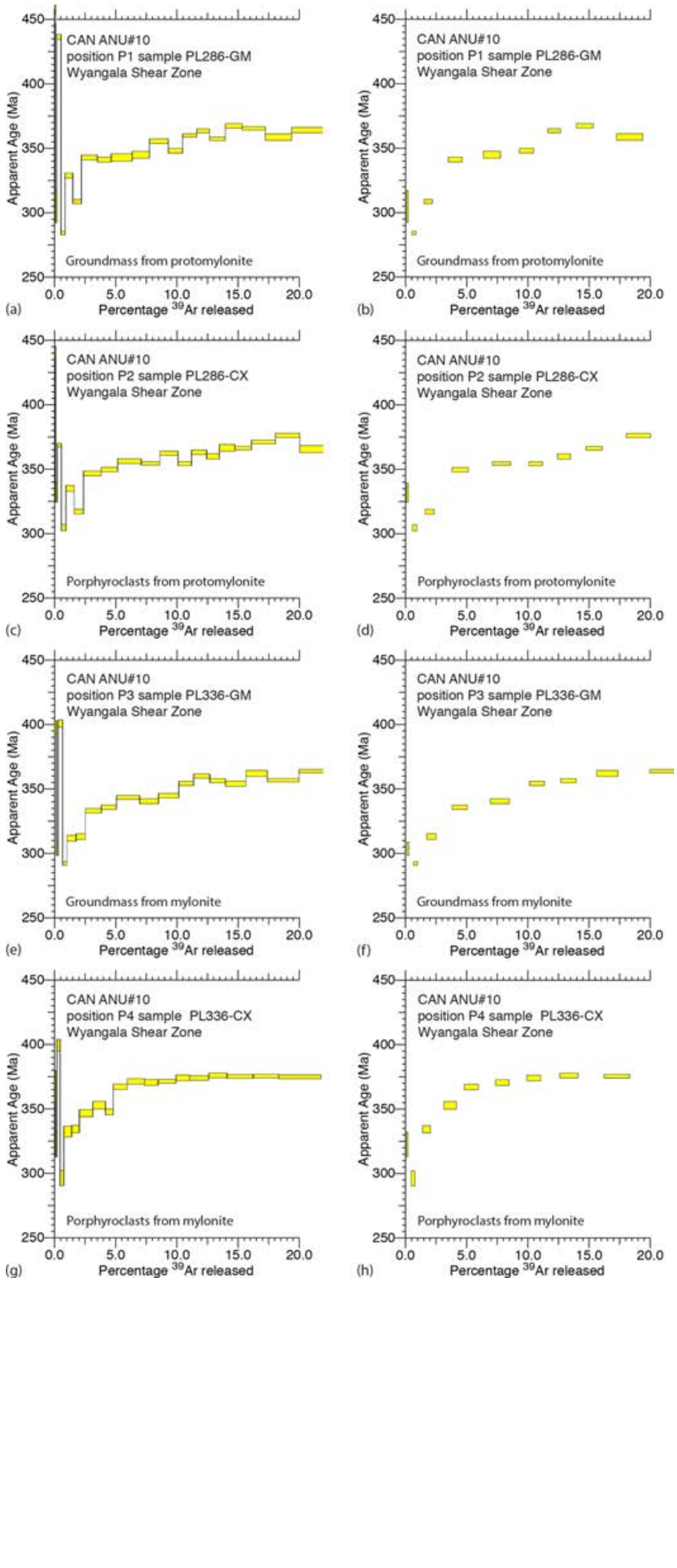

CAN ANU#10
position P1 sample PL286-GM
Wyangala Shear Zone
Groundmass from protomylonite
Apparent Age (Ma)
Percentage ^{39}Ar released
(a)
(b)
CAN ANU#10
position P2 sample PL286-CX
Wyangala Shear Zone
Porphyroclasts from protomylonite
(c)
(d)
CAN ANU#10
position P3 sample PL336-GM
Wyangala Shear Zone
Groundmass from mylonite
(e)
(f)
CAN ANU#10
position P4 sample PL336-CX
Wyangala Shear Zone
Porphyroclasts from mylonite
(g)
(h)

Figure 3

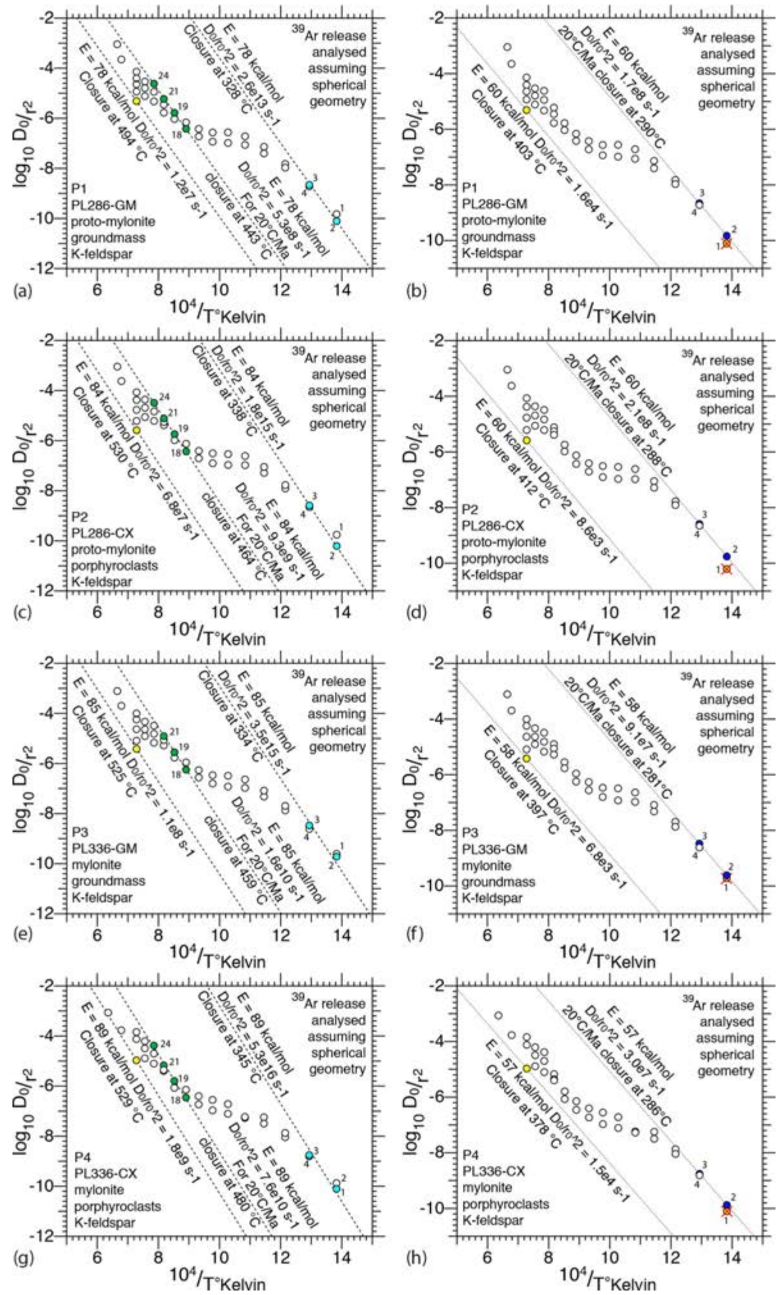

Figure 4

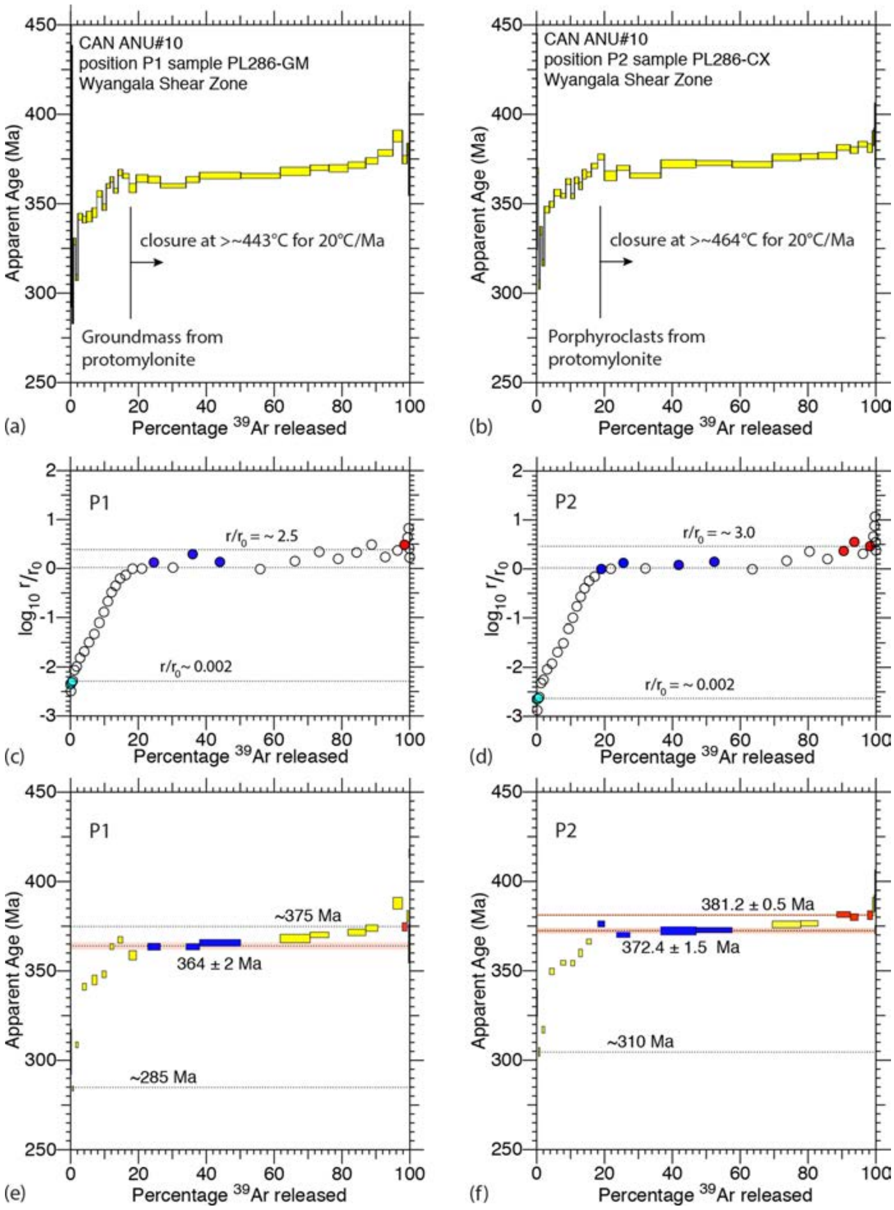

CAN ANU#10
position P1 sample PL286-GM
Wyangala Shear Zone
closure at >~443°C for 20°C/Ma
Groundmass from protomylonite
Apparent Age (Ma)
Percentage 39Ar released
(a)
CAN ANU#10
position P2 sample PL286-CX
Wyangala Shear Zone
closure at >~464°C for 20°C/Ma
Porphyroclasts from protomylonite
(b)
P1
r/r0 = ~ 2.5
r/r0 ~ 0.002
log10 r/r0
(c)
P2
r/r0 = ~ 3.0
r/r0 = ~ 0.002
(d)
P1
~375 Ma
364 ± 2 Ma
~285 Ma
(e)
P2
381.2 ± 0.5 Ma
372.4 ± 1.5 Ma
~310 Ma
(f)

Figure 5

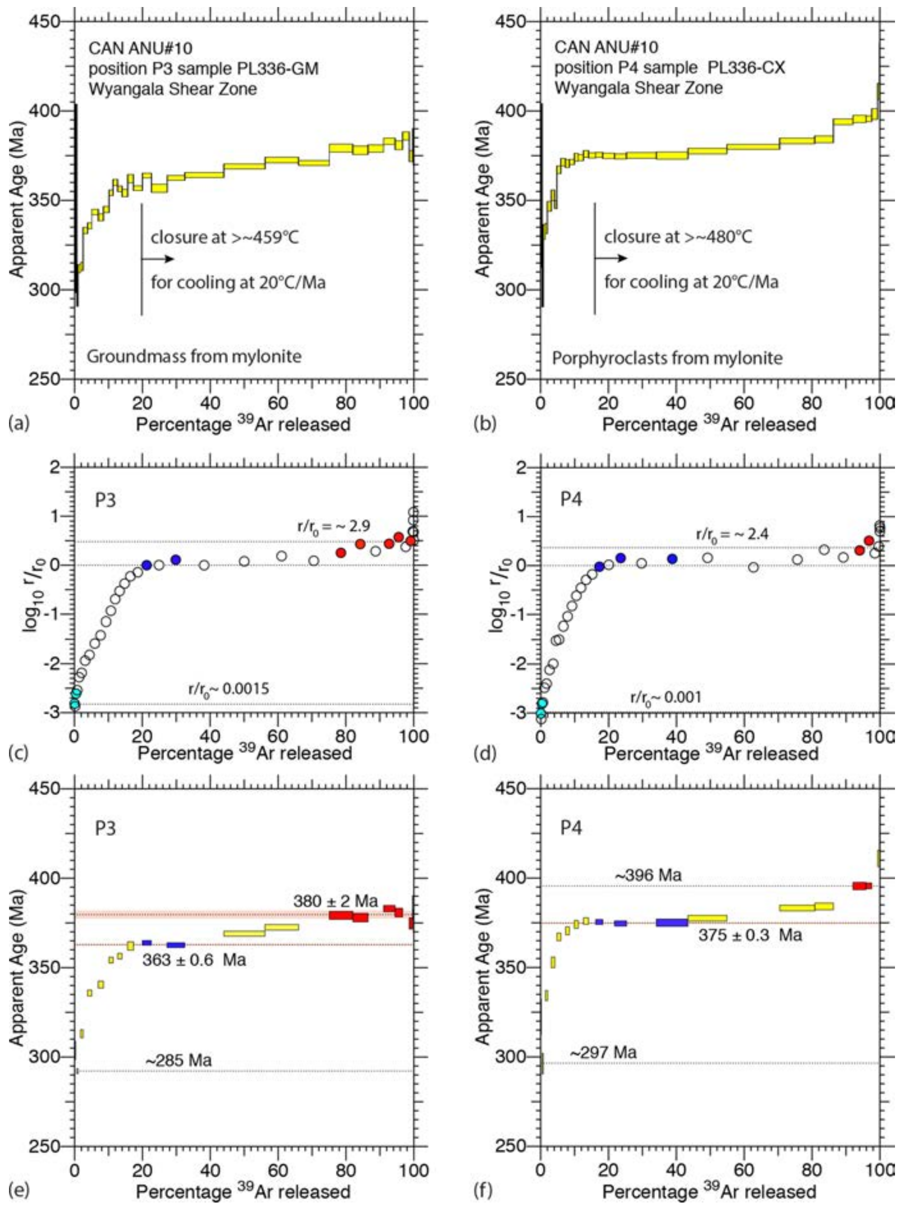
CAN ANU#10
position P3 sample PL336-GM
Wyangala Shear Zone
closure at >~459°C
for cooling at 20°C/Ma
Groundmass from mylonite
Apparent Age (Ma)
Percentage 39Ar released
(a)
CAN ANU#10
position P4 sample PL336-CX
Wyangala Shear Zone
closure at >~480°C
for cooling at 20°C/Ma
Porphyroclasts from mylonite
(b)
P3
r/r0 = ~ 2.9
r/r0 ~ 0.0015
log10 r/r0
(c)
P4
r/r0 = ~ 2.4
r/r0 ~ 0.001
(d)
P3
380 ± 2 Ma
363 ± 0.6 Ma
~285 Ma
(e)
P4
~396 Ma
375 ± 0.3 Ma
~297 Ma
(f)

Figure 6

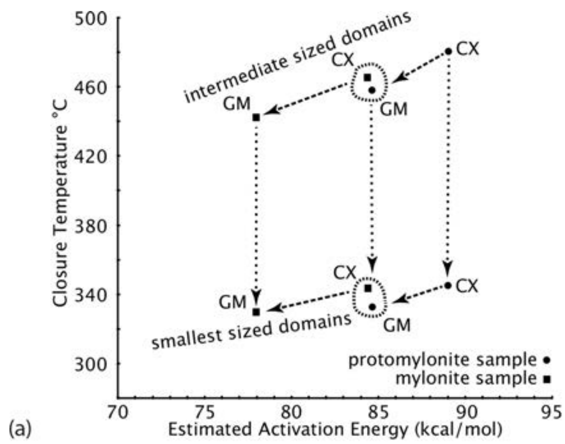
500
460
420
380
340
300
Closure Temperature °C
intermediate sized domains
CX
CX
GM
GM
CX
CX
GM
GM
smallest sized domains
protomylonite sample
mylonite sample
70
75
80
85
90
95
(a)
Estimated Activation Energy (kcal/mol)

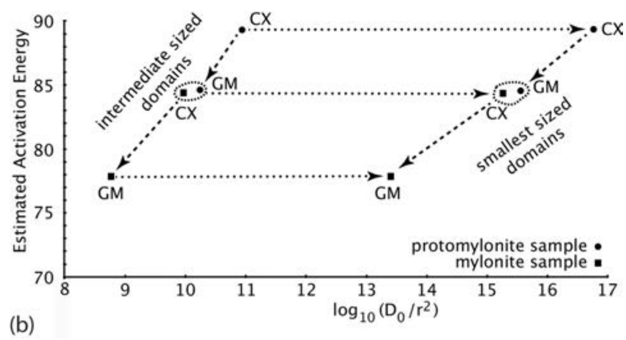
90
85
80
75
70
Estimated Activation Energy
intermediate sized domains
CX
CX
GM
CX
GM
CX
GM
GM
smallest sized domains
protomylonite sample
mylonite sample
8
9
10
11
12
13
14
15
16
17
$\log_{10}(D_0/r^2)$
(b)

Figure 7

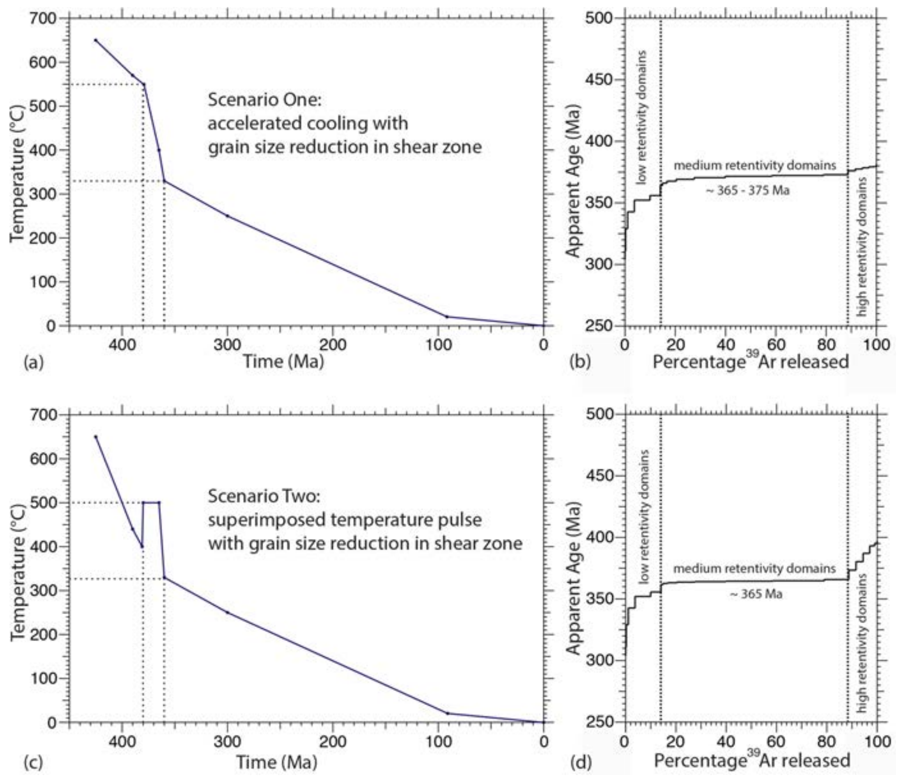

Scenario One:
accelerated cooling with
grain size reduction in shear zone
Temperature (°C)
Time (Ma)
(a)
Apparent Age (Ma)
Percentage ^{39}Ar released
low retentivity domains
medium retentivity domains
~ 365 - 375 Ma
high retentivity domains
(b)
Scenario Two:
superimposed temperature pulse
with grain size reduction in shear zone
Temperature (°C)
Time (Ma)
(c)
Apparent Age (Ma)
Percentage ^{39}Ar released
low retentivity domains
medium retentivity domains
~ 365 Ma
high retentivity domains
(d)

Figure 8